

Short Communication

Earth-Abundant SiX (X=S and Se) Monolayers as Promising Anode Materials for Lithium Ion Batteries, a First-Principles Study

Shijie Tan^{1,2} and Bo Dai^{1,*}

¹ State Key Laboratory of Environmental-friendly Energy Materials, Southwest University of Science and Technology, Mianyang, 621000, P.R. China

² Southwest Institute of Applied Magnetism, No. 268, North Binhe Road, Mianyang, People's Republic of China

*E-mail: daibo@swust.edu.cn (B.D.); jie1609@163.com (S.T)

Received: 18 August 2018 / Accepted: 19 September 2018 / Published: 5 November 2018

In this work, the adsorption energy, diffusion energy barrier and structural stability of Li on SiX (X=S and Se) monolayers were studied using density functional theory. The obtained adsorption energies were -3.41~-2.54 eV and -3.13 ~ -2.39 eV for Li absorbed on the SiS and SiSe monolayers, respectively. SiX (X=S and Se) monolayers show larger adsorption energies than those of other two-dimensional materials such as graphene and the MoO₂ monolayer. The diffusion of Li depends on the diffusion direction, showing an anisotropic diffusion behaviour. Li prefers to diffuse along the valley with the energy barriers of 0.27 and 0.28 eV on the SiS and SiSe monolayers, respectively. The structure is maintained to form LiSiX (X=S and Se). The characteristics of large adsorption energy, small Li diffusion energy barrier, and high structural stability indicate that SiX (X=S and Se) monolayers can be used as a potential anode for lithium ion batteries.

Keywords: SiX (X=S and Se) monolayer, lithium ion batteries, adsorption energy, diffusion energy, structural stability, density functional theory

1. INTRODUCTION

Graphite has been successfully and widely used as anode material for commercial lithium ion batteries (LIBs) due to its high structural stability [1]. However, the limited Li storage capacity (372 mAhg⁻¹) of graphite restricts its application in the high power devices required by electric vehicles. Graphene can be obtained by reducing the thickness of graphite to an atomic layer, and graphene and its composites show higher capacities of 600-1000 mAh/g [2, 3] than those of graphite [4]. The

increased capacity of graphene is due to its large surface-to-volume ratio that provides more adsorption sites for Li. This phenomenon inspired many researchers to explore other two-dimensional (2D) materials as electrode materials for the rechargeable ion batteries, such as boron carbon nitride nanosheets [5], V_2O_5 monolayer [6], MoS_2 monolayer [7-9], phosphorene monolayer [10-12] and other transition metal disulphide monolayers [13, 14]. These 2D materials have high capacities. Monolayer phosphorene has a capacity of 432.79 mAhg^{-1} with negligible volume changes [15]. The MoS_2 /graphene composite has a high specific capacity of $1225\text{-}1400 \text{ mAhg}^{-1}$ [16, 17], which is much higher than that of the current commercially used graphite. Since the diffusion path is shorter in 2D materials, facilitating Li diffusion, 2D electrode materials show higher charge/discharge rates and longer cycling lifetimes [18-22] and can thus satisfy the continuously increasing demand for high energy density and high power electronic devices. The diffusion barrier for Na on monolayer phosphorene is only 0.04 eV [23]. Other approaches such as introducing defects into the 2D materials [24] and piezo-electric field [25, 26] can be used to further improve the electrochemical performance of electrode materials. Although much progress has been made, searching for other new 2D materials that can be used as electrode materials for LIBs is still essential for satisfying the continuously rising demand for high energy power devices.

A good electrode material should have a large adsorption energy, small Li diffusion energy barrier, and high structural stability [27] to be used in a device that satisfies the large storage capacity, fast charging/discharging rate and safety requirement. Density functional theory (DFT) has been proven to be an effective method for predicting the electrochemical behaviour of electrode materials [28, 29]. Thus, computer simulations can greatly accelerate the rate of exploration of potential electrode materials. It is known that a monolayer phosphorene is a good anode for LIBs. Based on the "atomic transmutation" rule for designing new materials, in which one type of element is transmuted into its neighbouring elements in the periodic table, monolayer SiS can be obtained by changing P into Si and S. To date, efforts to search for the low cost, non-toxic, abundant and safe electrode materials for LIBs have faltered. Si and S are some of the most naturally abundant elements, which along with their low cost and non-toxic characteristics, makes them attractive candidate electrode materials for LIBs. To reveal whether nanolayered SiX (X=S and Se) materials can be used in LIBs, in the present paper, we systematically studied the adsorption and diffusion behaviour of Li on SiX (X=S and Se) monolayers using DFT simulations. It was shown that Li has a large adsorption energy on the SiX (X=S and Se) monolayer and a lower surface diffusion energy barrier, indicating that SiX (X=S and Se) monolayer can be used as a potential anode for LIBs.

2. COMPUTATIONAL DETAILS

First-principles calculations were performed with the SIESTA (Spanish Initiative for Effective Simulations with Thousands of Atoms) package [30]. Calculations for atomistic and electronic structure, adsorption and diffusion of Li on SiX (X=S and Se) monolayers were performed using DFT with the generalized gradient approximation (GGA) as parameterized by Perdew, Burke, and Ernzerhof (PBE) [31]. The electron-ion core interaction was described by non-local norm-conserving pseudo-

potentials [32]. The valence electron wave functions were expanded using a double- ζ basis set plus polarization functional with a cut-off of 200 Ry. The conjugate gradient method was used for the geometry optimizations, and the convergence condition was set to 0.01 eV/Å. Vacuum with the thickness of 30 Å was added above the monolayer to avoid the interaction between the periodically repeating layers.

3. RESULTS AND DISCUSSION

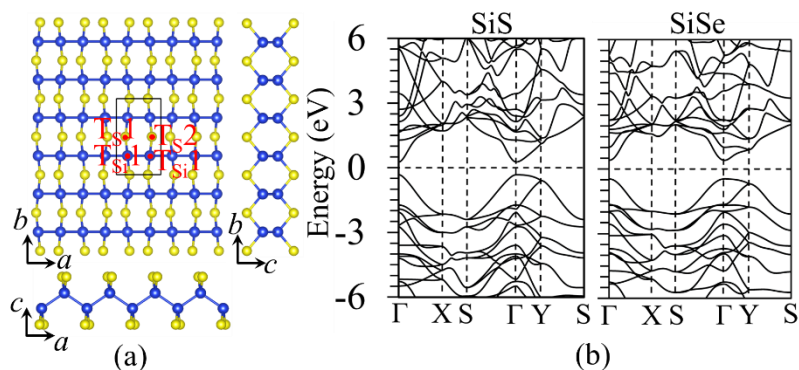


Figure 1. (a) Top and side views of a SiX (X=S and Se) monolayers. (b) Band structure of a SiX (X=S and Se) monolayer. T_{S1}, T_{S2}, T_{Si1} and T_{Si2} are the possible adsorption sites for lithium.

The SiX (X=S and Se) monolayers with the *Pm* symmetry were investigated. The relaxed atomistic structures viewed from different directions are shown in Fig. 1a. As seen from the *a-c* plane, the monolayer consists of Si zigzag chains along the *a* direction sandwiched by two atomic S (Se) layers. Each S (Se) atom is surrounded by two Si atoms, and each Si atom is surrounded by two S (Se) and two Si atoms.

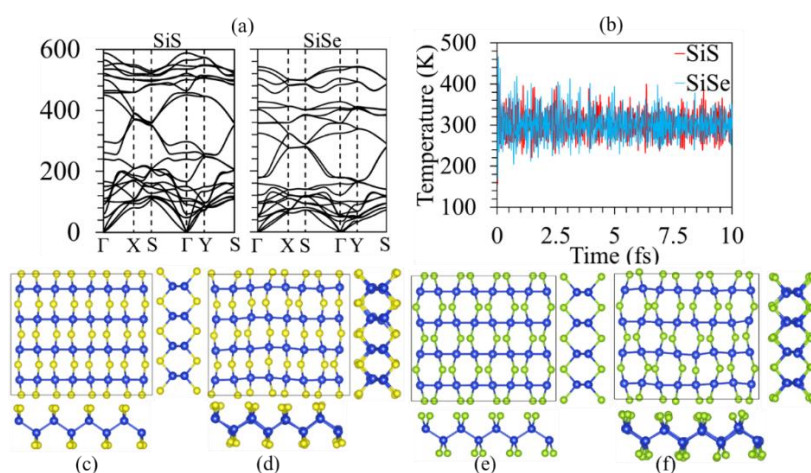


Figure 2. (a) Phonon dispersions of SiX (X=S and Se) monolayers. (b) Temperature evolution with simulation time of SiX (X=S and Se) monolayers at 300 K. (c) Initial and (d) relaxed atomic structures of SiS monolayer for 10 ps. (e) Initial and (f) relaxed atomic structures of SiSe monolayer for 10 ps.

As shown in Fig. 1a, the SiX (X=S and Se) monolayer has a rectangle unit cell. The calculated equilibrium lattice parameters are $a=3.912$ and $b=6.683$ Å for the SiS monolayer and $a=3.996$ and $b=6.940$ Å for the SiSe monolayer, and the larger lattice parameters of the SiSe monolayer compared to those of the SiS monolayer are due to the large radius of Se compared to S ion. The band structures of SiX (X=S and Se) monolayers are shown in Fig. 1b, and it is observed that both SiS and SiSe monolayers have direct bandgap at the Γ point, in agreement with other first-principles simulation results [33]. The obtained band gaps are 0.59 and 0.86 eV for SiS and SiSe monolayers, respectively.

The phonon dispersions of SiX (X=S and Se) monolayers calculated with the frozen phonon method [30] are shown in Fig. 2a. It is observed that there are no imaginary frequencies for both SiS and SiSe monolayers, and both the optical and acoustical branches have positive frequencies, indicating that both monolayers are reasonably stable. The thermal stability of the SiX (X=S and Se) monolayer was studied further using *ab initio* molecular dynamics (AIMD). A $4\times 2\times 1$ supercell containing 64 atoms was studied. A canonical NVT ensemble was used with the time step of 1.0 fs. Simulation times of up to 10 ps were tested to ensure that the conclusions are reliable. Fig. 2b shows the evolution of the simulation temperature as a function of simulation time. The temperature was kept at 300 K for the simulation. Figs. 2c and 2d show the initial and the final atomic structures of the SiS monolayer. After running for 10 ps at 300 K, no bond-breaking and geometric reconstruction was observed, and the SiS monolayer maintains its original structure except for a small vibration of Si and S atoms around their equilibrium crystalline sites. The evolution of the atomic configurations of the SiSe monolayer (Figs. 2e and 2f) show the same characteristics, indicating that SiS and SiSe monolayers are thermally stable at room temperature. Previous DFT calculations showed that SiX (X=S and Se) monolayers can be dynamically stable at temperatures up to 1000 K [33]. Thus, both the phonon dispersion curves and AIMD simulations demonstrate that the SiS and SiSe monolayers are stable with the *Pmma* symmetry structure.

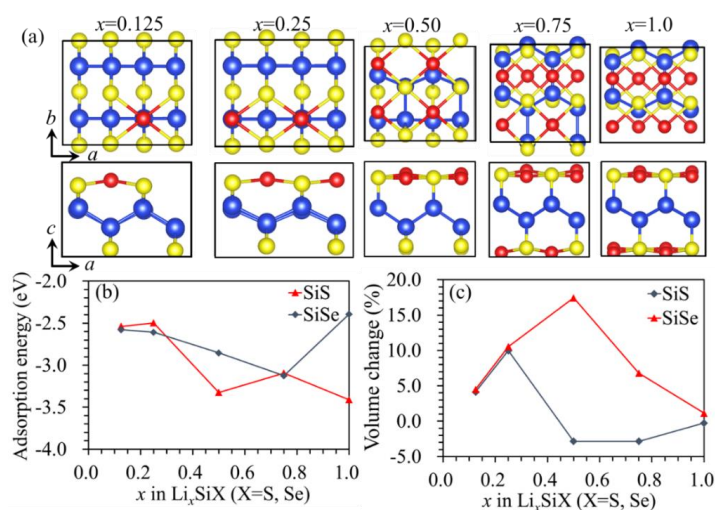


Figure 3. (a) Projected relaxed atomic configurations of Li_xSiS with $x=0.125$ -1.0 on a - b and a - c plane. (b) Adsorption energies as a function of the concentration of Li absorbed on SiX (X=S and Se) monolayers. (c) In-plane volume evolution as a function of the concentration of Li absorbed on SiX (X=S and Se) monolayers.

It is important to know the favourable adsorption sites for Li on SiX (X=S and Se) monolayers. As shown in Fig. 1, four high-symmetry adsorption sites were considered for Li adsorption on SiX (X=S and Se) monolayers, i.e., (i) the T_{S1} site, on top of the bottom S (Se) atom, (ii) the T_{S2} site, on top of the top S (Se) atom, (iii) the T_{Si1} site, on top of the bottom Si atom, and (iv) the T_{Si2} site, on top of the top Si atom. The adsorption energy was used to characterize the energy favourable adsorption sites and was calculated using equation (1):

$$E_{\text{ads}} = (E_{n\text{-Li-SiX}} - E_{\text{SiX}} - n \cdot E_{\text{Li}}) / n \quad (1)$$

where $E_{n\text{-Li-SiX}}$ is the total energy of SiX (X=S and Se) monolayers with n adsorbed lithium atoms, and E_{SiX} is the total energy of the supercell without the adsorbed lithium. E_{Li} is the energy of an isolated Li atom. According to equation (1), large negative adsorption energy means a favourable exothermic reaction between Li and the SiX (X=S and Se) monolayer. The calculated adsorption energies are -2.34 and -2.60 eV for Li adsorbed at the T_{S1} and T_{Si1} sites on the SiS monolayer, respectively. The T_{S2} and T_{Si2} sites are not stable sites for Li adsorption. It is observed that the Li adsorption at the T_{Si1} site is energetically favourable. The calculations also showed that the Li prefers to be adsorbed at the T_{Si1} site on the SiSe monolayer with the adsorption energy of -2.42 eV. High density Li adsorption on SiX (X=S and Se) monolayer to form Li_xSiX (X=S and Se) was also investigated, and the calculated adsorption energies are shown in Fig. 3b corresponding to with their atomic configurations shown in Fig. 3a. An exothermic reaction occurs between Li and the SiX (X=S and Se) monolayer, that shows no dependence on Li concentration, with all of the adsorption energies having negative values. It is observed from the atomic configurations that there was no bond breaking or bond reconstruction for all of the adsorbed Li, indicating that SiX (X=S and Se) monolayers can maintain their structural integrity upon lithiation. Since the thickness of monolayer structures is not well-defined, we used the in-plane volume change to characterize the volume evolution upon lithiation. The volume evolution as a function of lithium concentration is shown in Fig. 3c. The volume increased at the initial lithiation stage. For example, the volume increased by approximately 17.5% for the formation of Li_{0.5}SiSe. The volume change is very small for a high concentration of Li because the increased thickness is perpendicular to the monolayer. The volume changes are in the range -2.84%-9.98% and 1.17%-17.5% for the SiS and SiSe monolayers, respectively.

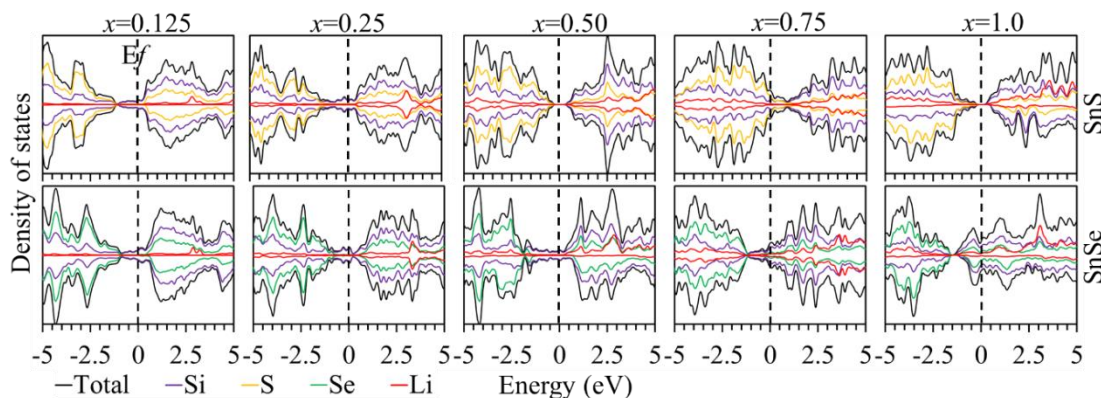


Figure 4. Projected density of states (PDOS) of lithiated SiS(Se) monolayers. The Fermi energy level (E_f) was set to 0.

Figure 4 shows the projected density of states (PDOS) of Li_xSiX ($X=\text{S}$ and Se). It is observed that the states near E_f (below and above the Fermi energy level) are contributed by the S (Se) and Si atoms, respectively. The Li states are located more than 2.5 eV above E_f , resulting in the donation of Li 2s electron to the SiX ($X=\text{S}$ and Se) monolayer, which leads to the strong adsorption of Li on SiX ($X=\text{S}$ and Se) monolayers.

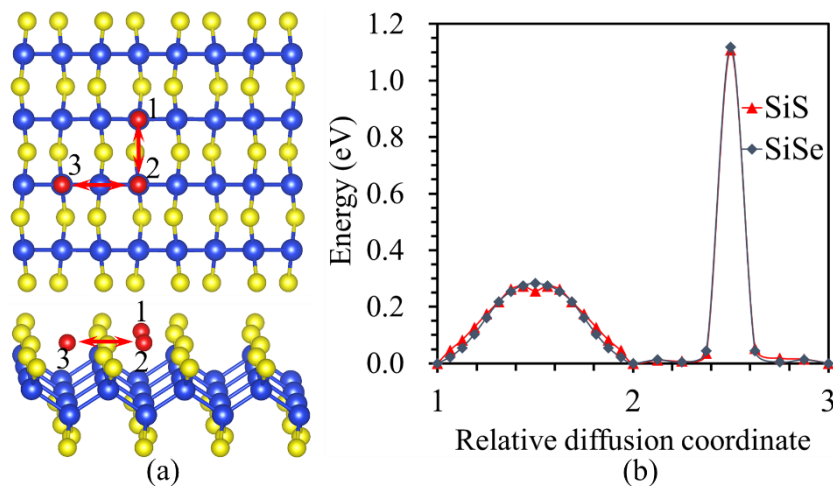


Figure 5. (a) Diffusion paths along and perpendicular to the valley formed by two lines of S atoms. (b) Energy barrier profile for Li diffusion on SiX ($X=\text{S}$ and Se) monolayers.

The ionic conductivity of Li in electrode materials is a key parameter for determining the charging/discharging rate of rechargeable ion batteries, and therefore, the diffusion energy barriers of Li on SiX ($X=\text{S}$ and Se) monolayers were investigated. As discussed above, Li prefers to be absorbed at the $T_{\text{Si}1}$ site on the monolayer, and therefore, the diffusion of Li from one $T_{\text{Si}1}$ site to the nearest neighbour $T_{\text{Si}1}$ site was studied. As shown in Fig. 5a, lithium can diffuse along or perpendicular to the valley formed by two lines of S atoms, and we denoted these two paths as path12 and path23. The diffusion energy profiles are shown in Fig. 5b. The energy barriers are 0.27 and 1.11 eV for Li diffusion on the SiS monolayer along path12 and path23, respectively. For Li, the diffusion values on the SiSe monolayer are 0.28 and 1.12 eV, respectively. The diffusion energy barriers for Li diffusion along path23 is approximately 4 times higher than the barrier for Li diffusion along path12. Thus, anisotropic diffusion behaviour is found for Li on SiX ($X=\text{S}$ and Se) monolayers, mainly due to the non-flat and puckered structure of SiX ($X=\text{S}$ and Se) monolayers.

Li shows strong adsorption with adsorption energies of -2.60 and -2.42 eV for Li on the SiS and SiSe monolayers, respectively, and the absolute values of the adsorption energy is much larger than that of Li absorbed on graphene (-1.23 eV) [34], and on the MoS_2 monolayer (-2.01 eV) [7]. The relatively low diffusion barriers of -2.60 and -2.42 eV for Li on the SiS and SiSe monolayers are comparable to the diffusion barriers found for other two-dimensional materials, such as for Li on graphene (0.26 eV) [34] and on a black phosphorus monolayer (0.36 eV) [35]. The structure is stable upon lithiation. All of these results indicate that SiX ($X=\text{S}$ and Se) monolayers can be potentially used

as anodes for LIBs. Since there is no available electrochemical data to compare with DFT calculations, further experimental validation is necessary to realize SiX (X=S and Se) monolayers as anodes for LIBs.

4. CONCLUSION

In conclusion, the structural and electronic properties of the SiX (X=S and Se) monolayers were investigated using first-principles calculations. Adsorption and diffusion of Li on the SiX (X=S and Se) monolayer were also revealed by the simulations. The adsorption energies were in the range of -3.41 ~ -2.54 eV and -3.13 ~ -2.39 eV for Li absorbed on the SiS and SiSe monolayers, respectively. SiX (X=S and Se) monolayer maintain their structural integrity to form Li SiX (X=S and Se) with volume changes in the range -2.84%-9.98% and 1.17%-17.5% for the SiS and SiSe monolayers, respectively. An anisotropic diffusion behaviour was found for Li on SiX (X=S and Se) monolayers, with lithium preferring to diffuse in the valley with the energy barriers of 0.27 and 0.28 eV for Li on the SiS and SiSe monolayers, respectively. All of the results indicate that SiX (X=S and Se) monolayers are promising materials for anodes of LIBs.

ACKNOWLEDGEMENT

We thank the Programme for Young Science and Technology Innovation Teams of Sichuan Province (2017TD0020) and the Key Research and Development programme of Sichuan Province (Grant Number: 2017GZ0166).

References

1. J.K.E. Yoo, E. Hosono, H.S. Zhou, and T. Kudo, *Nano Lett.*, 8 (2008) 2277-2282.
2. G. Wang, X. Shen, J. Yao, and J. Park, *Carbon*, 47 (2009) 2049-2053.
3. D. Wang, R. Kou, D. Choi, Z. Yang, Z. Nie, J. Li, L.V. Saraf, D. Hu, J. Zhang, G.L. Graff, J. Liu, M.A. Pope, and I.A. Aksay, *ACS Nano*, 4 (2010) 1587-1595.
4. J.R. Dahn, T. Zheng, Y.H. Liu, and J.S. Xue, *Science*, 270 (1995) 590-593.
5. W.W. Lei, S. Qin, D. Liu, D. Portehault, Z.W. Liu, and Y. Chen, *Chem. Commun.*, 49 (2013) 352-354.
6. Z. Wang, Q. Su, and H. Deng, *Phys. Chem. Chem. Phys.*, 15 (2013) 8705-8709.
7. X. Sun, Z. Wang, and Y.Q. Fu, *Sci. Rep.*, 5 (2015) 18712.
8. X. Sun, Z. Wang, Z. Li, and Y.Q. Fu, *Sci. Rep.*, 6 (2016) 26666.
9. W. Shi, Z. Wang, Z. Li, and Y.Q. Fu, *Mater. Chem. Phys.*, 183 (2016) 392-397.
10. W. Li, Y. Yang, G. Zhang, and Y.W. Zhang, *Nano Lett.*, 15 (2015) 1691-1697.
11. X. Sun and Z. Wang, *Appl. Surf. Sci.*, 427 (2018) 189-197.
12. W. Jin, Z. Wang, and Y.Q. Fu, *J. Mater. Sci.*, 51 (2016) 7355-7360.
13. X. Sun and Z. Wang, *Appl. Surf. Sci.*, 455 (2018) 911-918.
14. X. Sun and Z. Wang, *Beilstein J. Nanotechnology*, 8 (2017) 2711-2718.
15. S. Zhao, W. Kang, and J. Xue, *J. Mater. Chem. A*, 2 (2014) 19046-19052.
16. F.Y. Xiong, Z.Y. Cai, L.B. Qu, P.F. Zhang, Z.F. Yuan, O.K. Asare, W.W. Xu, C. Lin, and L.Q. Mai, *ACS Appl. Mater. Interf.*, 7 (2015) 12625-12630.

17. X.Y. Yu, H. Hu, Y.W. Wang, H.Y. Chen, and X.W. Lou, *Angew. Chem. Int. Edit.*, 54 (2015) 7395-7398.
18. Y. Jing, E.O. Ortiz-Quiles, C.R. Cabrera, Z. Chen, and Z. Zhou, *Electrochim. Acta*, 147 (2014) 392-400.
19. M. Mortazavi, C. Wang, J. Deng, V.B. Shenoy, and N.V. Medhekar, *J. Power Sources*, 268 (2014) 279-286.
20. V.V. Kulish, O.I. Malyi, M.-F. Ng, P. Wu, and Z. Chen, *RSC Adv.*, 3 (2013) 4231.
21. Q.F. Li, C.G. Duan, X.G. Wan, and J.L. Kuo, *J. Phys. Chem. C*, 119 (2015) 8662-8670.
22. V.V. Kulish, O.I. Malyi, M.F. Ng, Z. Chen, S. Manzhos, and P. Wu, *Phys. Chem. Chem. Phys.*, 16 (2014) 4260-4267.
23. V.V. Kulish, O.I. Malyi, C. Persson, and P. Wu, *Phys. Chem. Chem. Phys.*, 17 (2015) 13921-13928.
24. X. Sun, Z. Wang, and Y.Q. Fu, *Carbon*, 116 (2017) 415-421.
25. W.W. Shi, Z.G. Wang, and Y.Q. Fu, *J. Phys. D: Appl. Phys.*, 50 (2017) 405303.
26. Z.G. Wang, Z.J. Li, and Y.Q. Fu, *ChemElectroChem*, 4 (2017) 1523-1527.
27. D. Datta, J. Li, N. Koratkar, and V.B. Shenoy, *Carbon*, 80 (2014) 305-310.
28. Z. Wang, Y. He, M. Gu, Y. Du, S.X. Mao, and C. Wang, *ACS Appl. Mater. Interf.*, 8 (2016) 24567-24572.
29. Z. Wang, M. Gu, Y. Zhou, X. Zu, J.G. Connell, J. Xiao, D. Perea, L.J. Lauhon, J. Bang, S. Zhang, C. Wang, and F. Gao, *Nano Lett.*, 13 (2013) 4511-4516.
30. J. M. Soler, E. Artacho, J. D. Gale, Alberto Garcia, J. Junquera, P. Ordejon and D. Sanchez-Portal, *J. Phys. Condens. Matter.*, 14 (2002) 2745.
31. K.B. John and P. Perdew, Matthias Ernzerhof, *Phys. Rev. Lett.*, 77 (1996) 3865-3868.
32. N. Troullier and J.L. Martins, *Phys. Rev. B*, 43 (1991) 8861-8869.
33. J.H. Yang, Q. Yuan, H.X. Deng, S.H. Wei, and B.I. Yakobson, *J. Phys. Chem. C* 121 (2017) 123-128
34. Z. Wang, *ACS Appl. Mater. Interf.*, 9 (2017) 15893-15897.
35. H.R. Jiang, W. Shyy, M. Liu, L. Wei, M.C. Wu, and T.S. Zhao, *J. Mater. Chem. A*, 5 (2017) 672-679